Virus Molecular Building Blocks

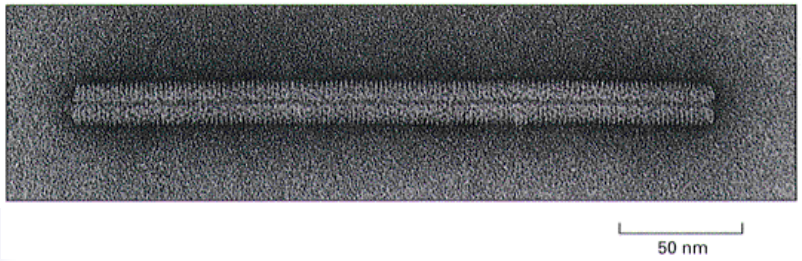

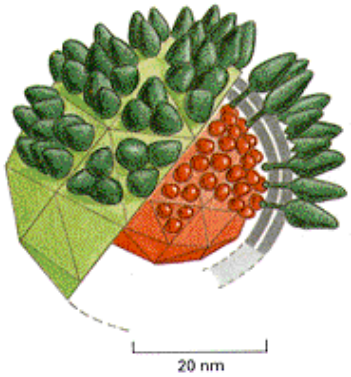

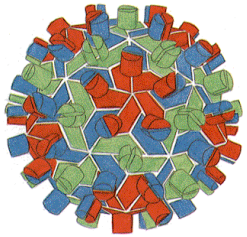

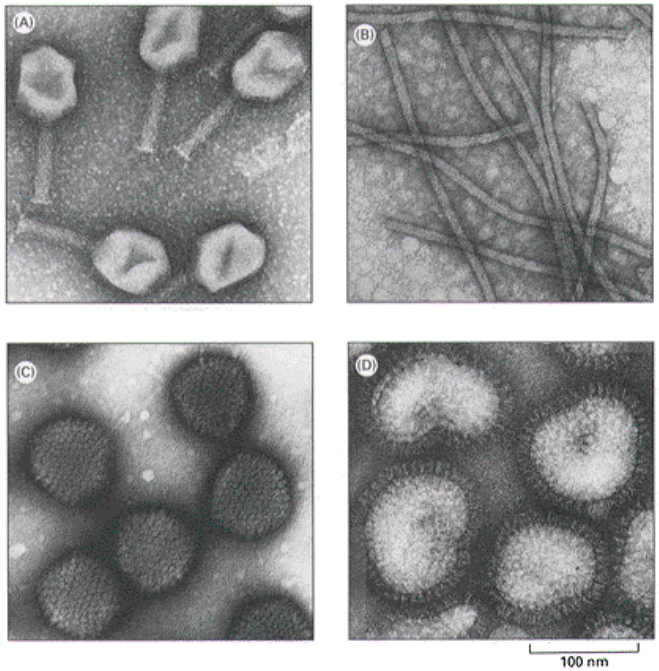

- Viral MBBs
- Organize nanomaterials
- 2D and 3D crystal lattices
- *In vitro* evolution of new functions
- Encapsulation
- Bioactive programmable nanomachines

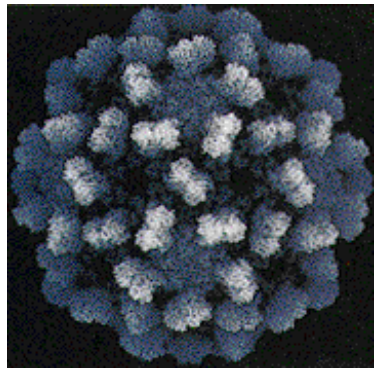

Selection of peptides with semiconductor binding specificity for directed nanocrystal assembly

NATURE | VOL 405 | 8 JUNE 2000 | 665

Sandra R. Whaley*, D. S. English*, Evelyn L. Hu†, Paul F. Barbara*‡ & Angela M. Belcher*‡

In biological systems, organic molecules exert a remarkable level of control over the nucleation and mineral phase of inorganic materials such as calcium carbonate and silica, and over the assembly of crystallites and other nanoscale building blocks into complex structures required for biological function[1–4]. This ability to direct the assembly of nanoscale components into controlled and sophisticated structures has motivated intense efforts to develop assembly methods that mimic or exploit the recognition capabilities and interactions found in biological systems[5–10]. Of particular value would be methods that could be applied to materials with interesting electronic or optical properties, but natural evolution has not selected for interactions between biomolecules and such materials. However, peptides with limited selectivity for binding to metal surfaces and metal oxide surfaces have been successfully selected[10,11]. Here we extend this approach and show that combinatorial phage-display libraries can be used to evolve peptides that bind to a range of semiconductor surfaces with high specificity, depending on the crystallographic orientation and composition of the structurally similar materials we have used. As electronic devices contain structurally related materials in close proximity, such peptides may find use for the controlled placement and assembly of a variety of practically important materials, thus broadening the scope for 'bottom-up' fabrication approaches.

- Biological systems control mineral nucleation
  - Calcium carbonate
  - Silica
  - Calcium phosphate
  - Etc.
- Can we mimic or exploit these abilities for nanotech applications?
- What about other materials?
  - Metals?
  - Metal oxides?
  - Semiconductors?

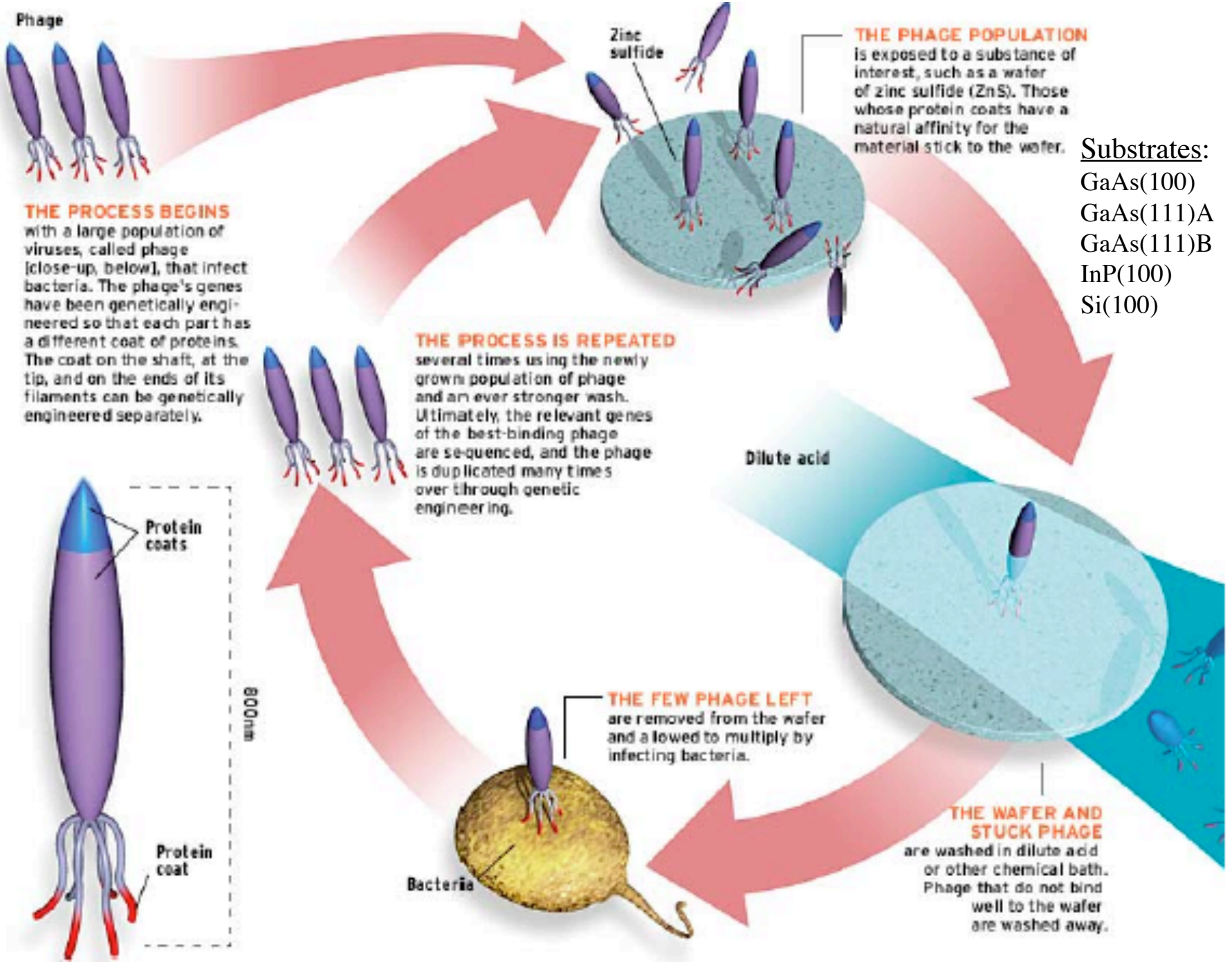

Substrates:
GaAs(100)
GaAs(111)A
GaAs(111)B
InP(100)
Si(100)

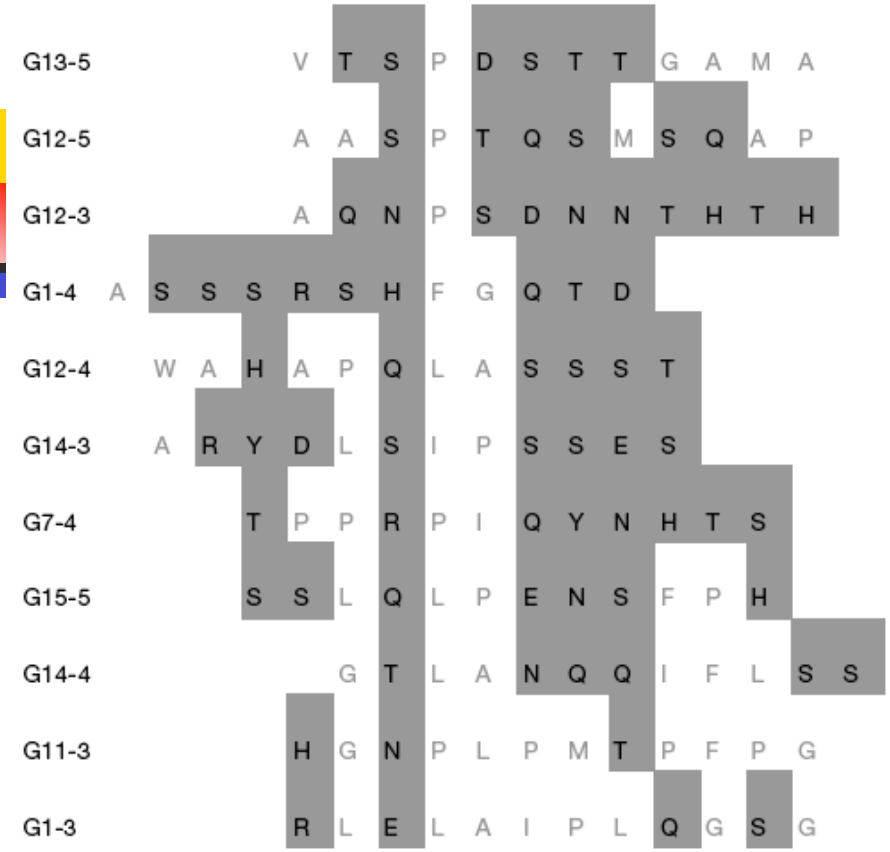

Figure 1 Selected amino-acid sequences of randomized peptide inserts. Here we show partial amino-acid sequences from clones that bound to GaAs(100). These sequences have amino acids with functional groups that can donate electrons to the GaAs surface (shaded areas). Serine (S) and threonine (T) both have hydroxyl side chains that differ by one carbon. Asparagine (N) and glutamine (Q) both have amine-bearing side chains that differ by one carbon. Non-polar amino acids are indicated by grey lettering. The clones were named as follows: G1-3 was the first clone selected from GaAs (100) during the third round of selection.

- Phage library
  - 12 random AA fused to M13 pIII coat protein (3-5 copies/phage)
- Selection
  - Bind, elute, million-fold amplification, reselect with increased stringency
- Substrates
  - Crystal face preferences
  - Gallium-rich (111)A
  - Arsenic-rich (111)B
- Peptides
  - Selected clones were enriched in uncharged non-polars (S,T) and Lewis bases (N,Q)

- XPS of Au 4f (panels a&b) Ga 2p (panel c)

Surface-Phage-Ab-biotin-SA-Au (20nm)

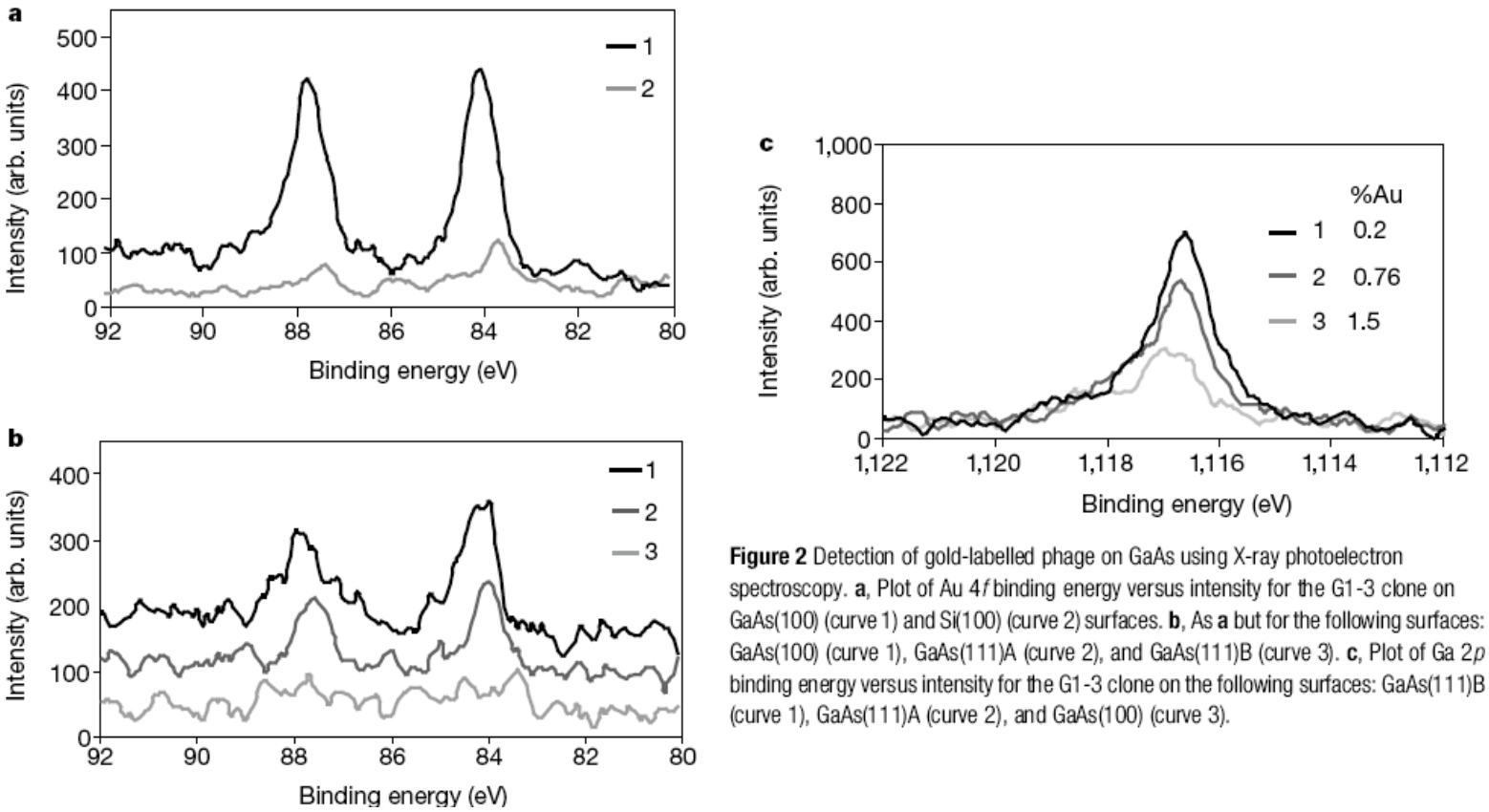

Figure 2 Detection of gold-labelled phage on GaAs using X-ray photoelectron spectroscopy. **a**, Plot of Au 4*f* binding energy versus intensity for the G1-3 clone on GaAs(100) (curve 1) and Si(100) (curve 2) surfaces. **b**, As **a** but for the following surfaces: GaAs(100) (curve 1), GaAs(111)A (curve 2), and GaAs(111)B (curve 3). **c**, Plot of Ga 2*p* binding energy versus intensity for the G1-3 clone on the following surfaces: GaAs(111)B (curve 1), GaAs(111)A (curve 2), and GaAs(100) (curve 3).

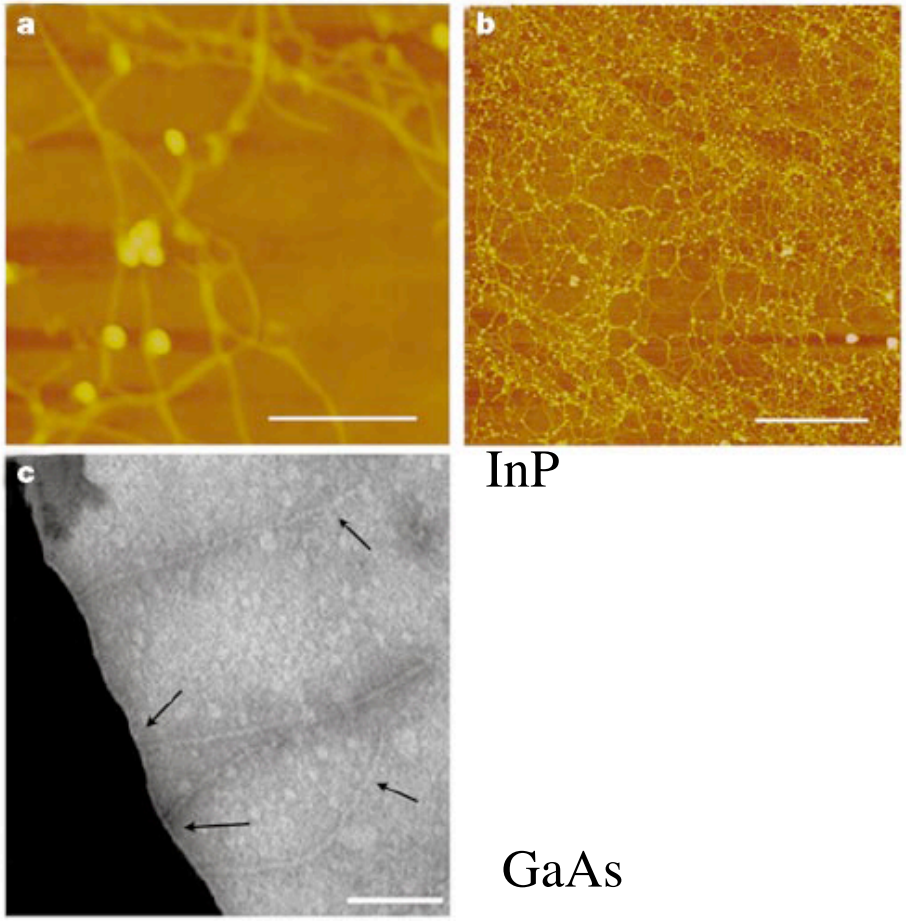

Figure 3 AFM and TEM analysis of peptide–semiconductor recognition. **a**,**b**, AFM images of G1-3 phage bound to an InP(100) substrate. **a**, Individual phage and their attached Au nanoparticles. Scale bar, 250 nm. **b**, Image showing the uniformity of phage coverage on the InP surface. Scale bar, 2.5 μm. **c**, TEM image of G1-3 phage recognition of GaAs. Individual phage particles are indicated with arrows. Scale bar, 500 nm.

- AFM and TEM of: **Surface-Phage-Ab-biotin-SA-Au**
- GaAs selected phage binds to InP which has a zinc-blende structure, isostructural with GaAs but with increased ionic character in In-P bond.

- A. control Ab rhodamine (no phage)
- B. Selectivity of rhodamine labeled G12-3 for GaAs vs SiO_2
- C. Selectivity of gold labeled G12-3 for GaAs vs AlGaAs

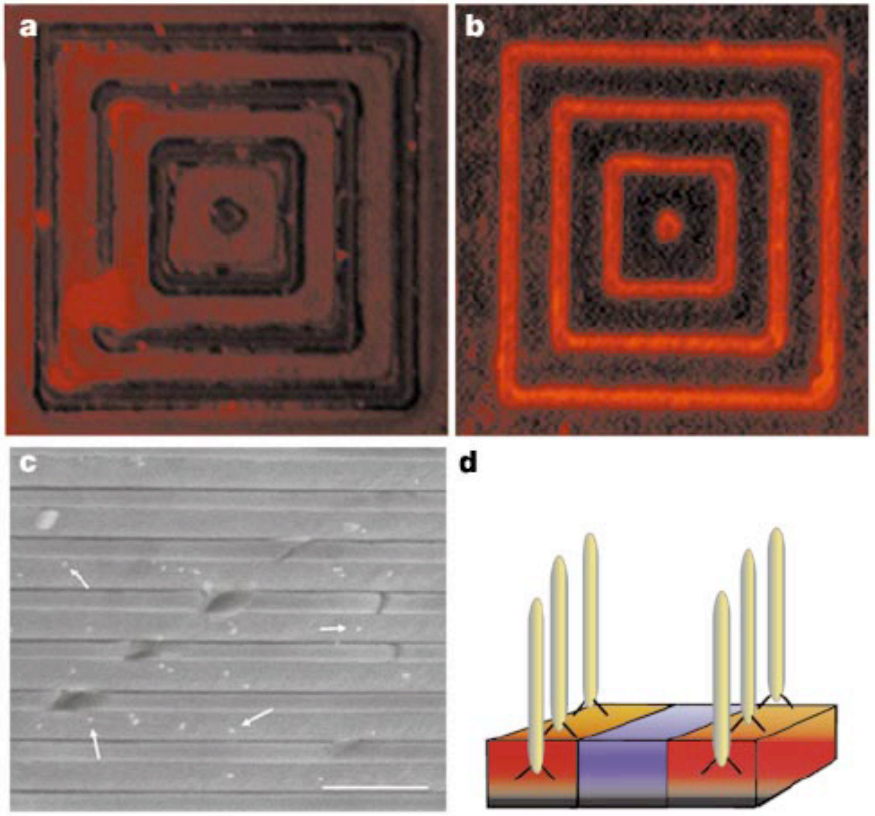

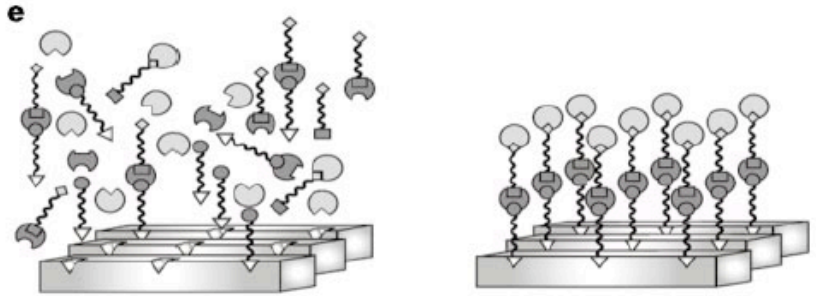

Figure 4 Phage recognition of semiconductor heterostructures. **a**–**c**, Fluorescence images related to GaAs recognition by phage. **a**, Control experiment: no phage is present, but primary antibody and streptavidin-tetramethyl rhodamine (TMR) are present. **b**, The GaAs clone G12-3 was interacted with a substrate patterned with 1-μm GaAs lines and 4-μm SiO_2 spaces. The phage were then fluorescently labelled with TMR. The G12-3 clone specifically recognized the GaAs and not the SiO_2 surface; scale bar, 4 μm. A diagram of this recognition process is shown in **d**, in which phage specifically attach to one semiconductor rather than another, in a heterostructure. **c**, An SEM image of a heterostructure containing alternating layers of GaAs and $Al_{0.98}Ga_{0.02}As$, used to demonstrate that this recognition is element-specific. The cleaved surface was interacted with G12-3 phage, and the phage was then tagged with 20-nm gold particles. These nanoparticles (shown arrowed in **c**) are located on GaAs and not AlGaAs layers. Scale bar, 500 nm. **e**, Diagram illustrating the use of this specificity to design nanoparticle heterostructures using proteins with multiple recognition sites.

Ordering of Quantum Dots Using Genetically Engineered Viruses

Seung-Wuk Lee, Chuanbin Mao, Christine E. Flynn, Angela M. Belcher*†

A liquid crystal system was used for the fabrication of a highly ordered composite material from genetically engineered M13 bacteriophage and zinc sulfide (ZnS) nanocrystals. The bacteriophage, which formed the basis of the self-ordering system, were selected to have a specific recognition moiety for ZnS crystal surfaces. The bacteriophage were coupled with ZnS solution precursors and spontaneously evolved a self-supporting hybrid film material that was ordered at the nanoscale and at the micrometer scale into ~72-micrometer domains, which were continuous over a centimeter length scale. In addition, suspensions were prepared in which the lyotropic liquid crystalline phase behavior of the hybrid material was controlled by solvent concentration and by the use of a magnetic field.

3 MAY 2002 VOL 296 SCIENCE **892**

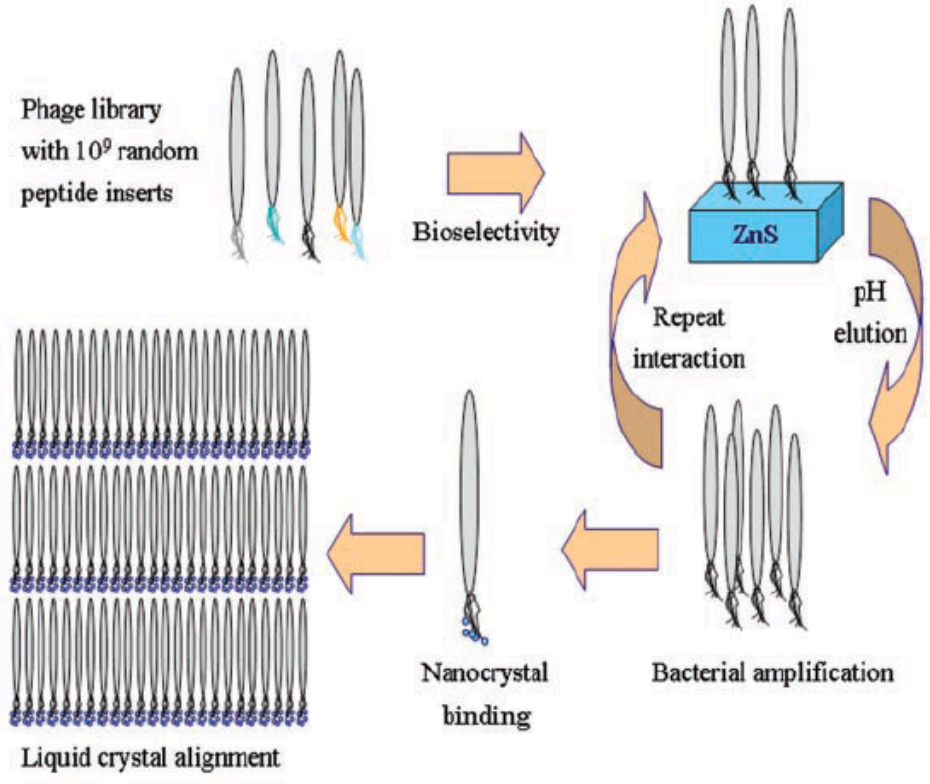

Polarized optical microscopy **Differential interference contrast imaging**

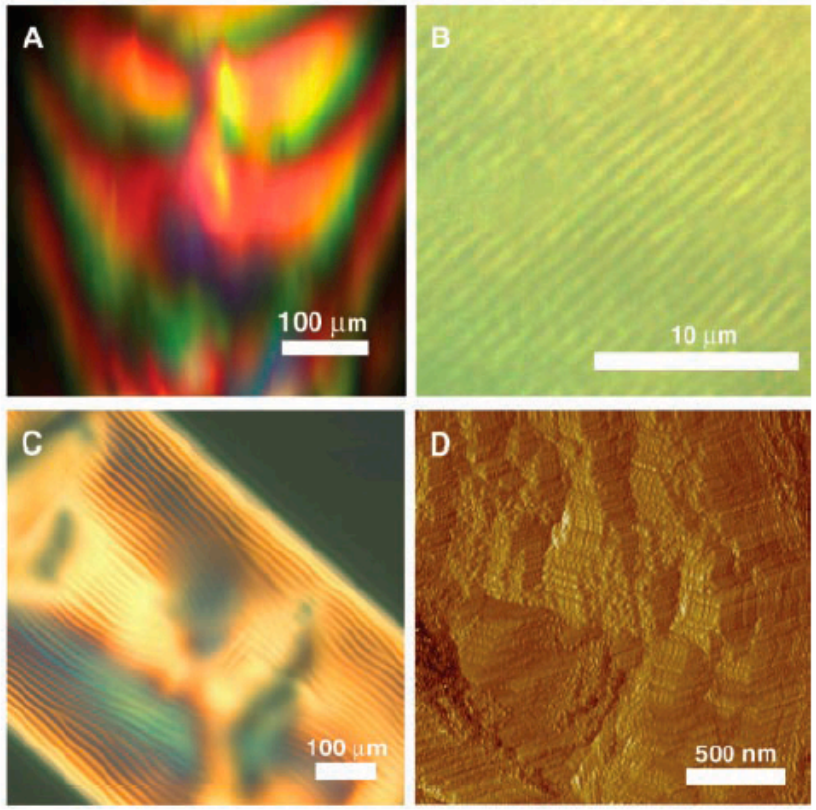

Fig. 1 (left). Schematic diagram of the process used to generate nanocrystal alignment by the phage display method. **Fig. 2 (right).** Characterization of the liquid crystalline suspensions of A7 phage–ZnS nanocrystals (A7-ZnS) and cast film. (**A**) POM image of a smectic suspension of A7-ZnS at a concentration of 127 mg/ml. (**B**) A DIC filter brought out dark and bright periodic stripes (~1 µm) that show constructive and destructive interference patterns generated from parallel aligned smectic layers in the A7-ZnS suspension. (**C**) The characteristic fingerprint texture of the cholesteric phase of an A7-ZnS suspension (76 mg/ml). (**D**) AFM micrograph of a cast film from an A7-ZnS suspension (~30 mg/ml) showing close-packed structures of the A7 phage particles.

Liquid crystals

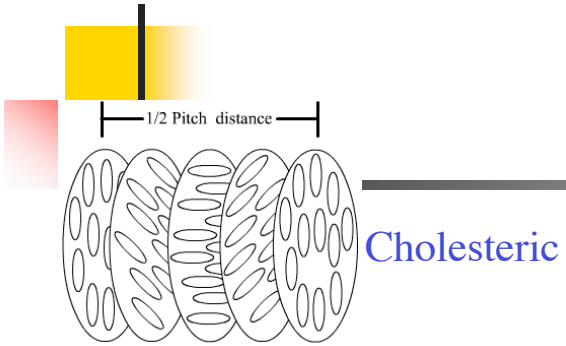

Cholesteric

Smectic

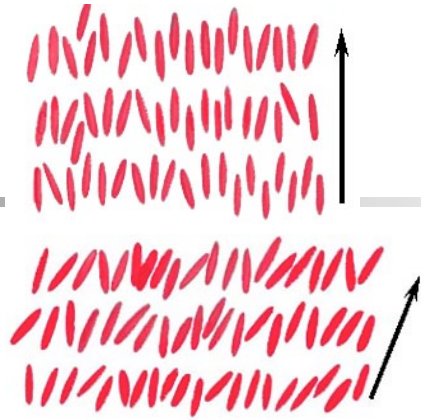

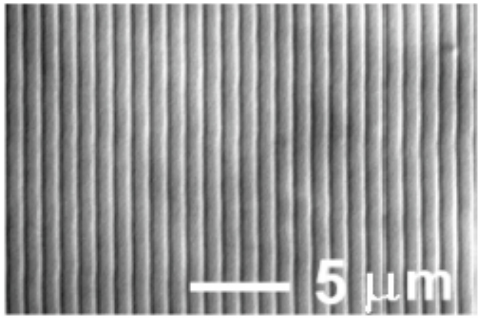

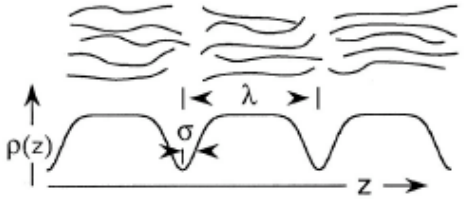

FIG. 1. Top: DIC optical micrograph of the fd smectic. The high contrast narrow black-white lines are the gaps between smectic layers. The half-width of the gap σ between layers is 90 nm and the smectic layer spacing λ is 920 nm. The particles lie in the plane of the photo and are oriented perpendicular to the smectic planes. Bottom: The upper part of the sketch shows the flexible fd molecules in the smectic phase. The lower portion is a plot of the fd density distribution $\rho(z)$ given in Eq. (1), as a function of distance z perpendicular to the smectic layers.

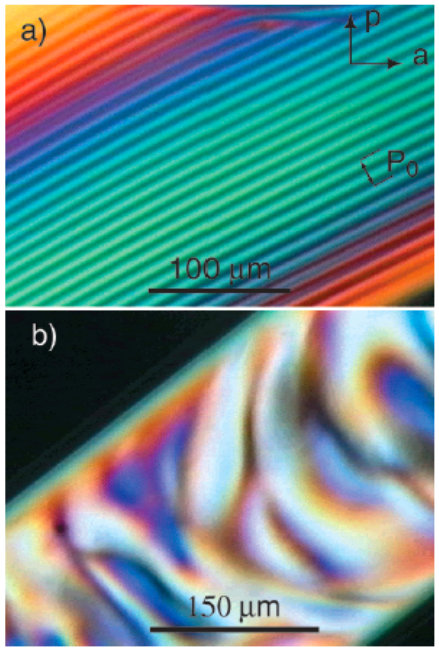

Figure 1. Typical texture of a cholesteric phase of a liquid crystalline sample of *fd* observed with polarization microscopy. Dark lines correspond to regions where the rods are perpendicular to the plane of the paper and bright lines correspond to regions where rods are in the plane of paper. The length of the cholesteric pitch (P_0) spans two bright and two dark lines as indicated in the micrograph. The concentration of the *fd*

Nematic

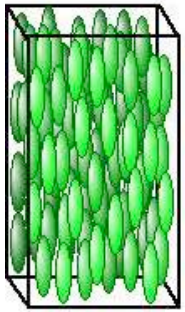

- Nematic phase
  - no positional order but tend to point in the same direction
- Smectic phase
  - orientational order of nematics, but also tend to align themselves in layers (from Greek word for “soap”)
- Cholesteric phase
  - many chiral nematic slabs of infinitesimal thickness and helical rotation of director layer to layer. Not to be confused with the planar arrangement found in smectic phases

(0.01% diluted sample)

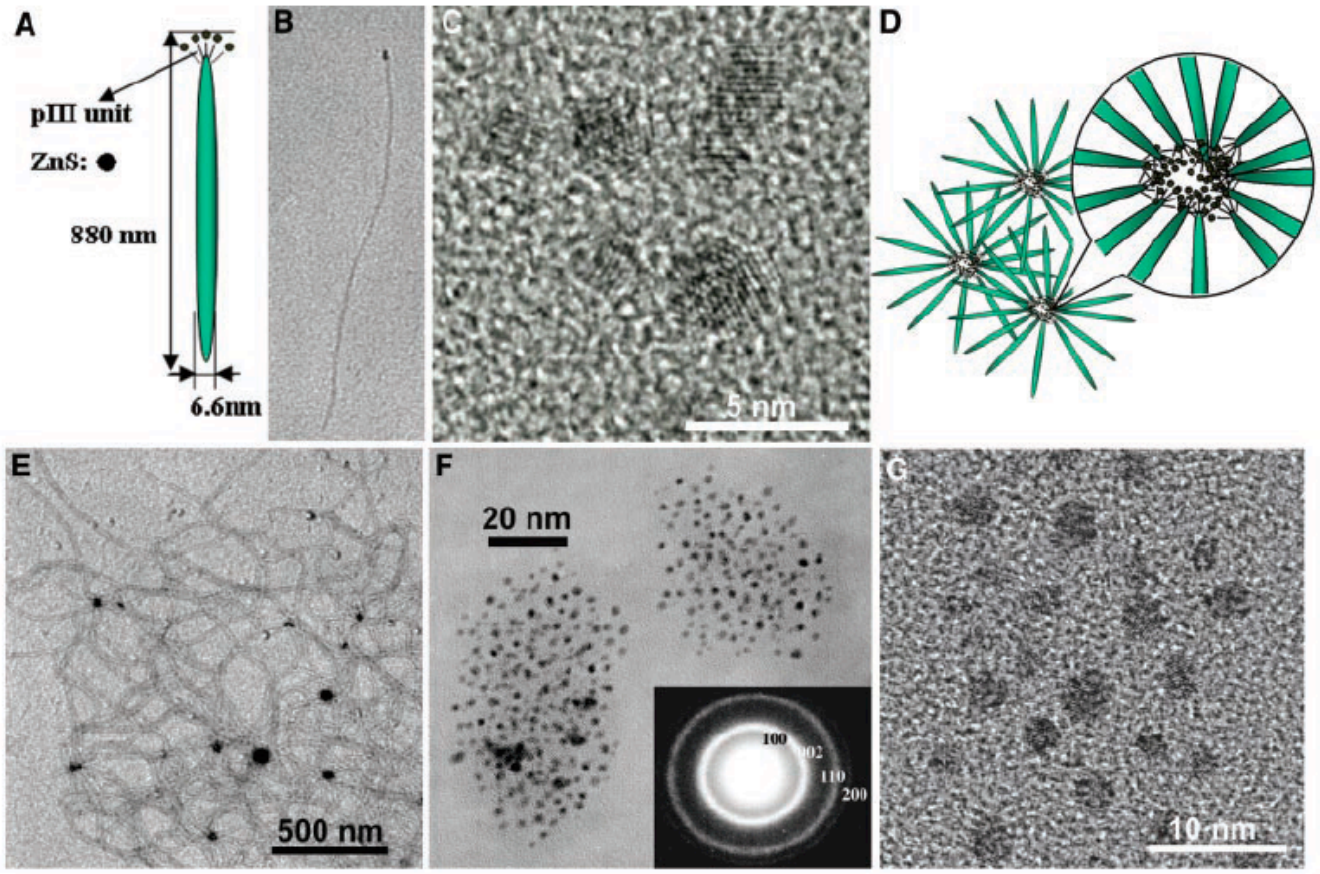

Fig. 3. Characterization of the dilute A7-ZnS suspension using TEM. (**A**) Schematic diagram of the individual A7 phage and ZnS nanocrystals. The pIII peptide unit and the ZnS nanocrystal bound to A7 phage are not drawn to scale. (**B**) TEM image of an individual A7 phage (880 nm in length) and ZnS nanocrystals, stained with 2% uranyl acetate. (**C**) High-resolution TEM image of 0.01% A7-ZnS suspension, showing lattice fringe images of five wurtzite ZnS nanocrystals. The *d* spacing of the nanocrystals was 0.22 nm, corresponding to (102) plane. (**D**) A schematic diagram of the micelle-like structures, in which ZnS nanocrystal aggregates are surrounded by A7 phage. (**E**) Low-resolution TEM image of 0.1% dilute A7-ZnS smectic suspension, showing micelle-like aggregates of ZnS nanocrystals surrounded by A7 phage after staining. (**F**) The same sample from (E) before staining shows that 100 to 150 nanocrystals formed aggregates. The inset shows a selected area electron diffraction pattern of the nanocrystal aggregates, confirming crystalline wurtzite ZnS structures. (**G**) High-resolution TEM image of 0.1% A7-ZnS suspension showing lattice fringe images of wurtzite ZnS nanocrystals. The *d* spacing of the nanocrystals was 0.22 nm, corresponding to (102) plane.

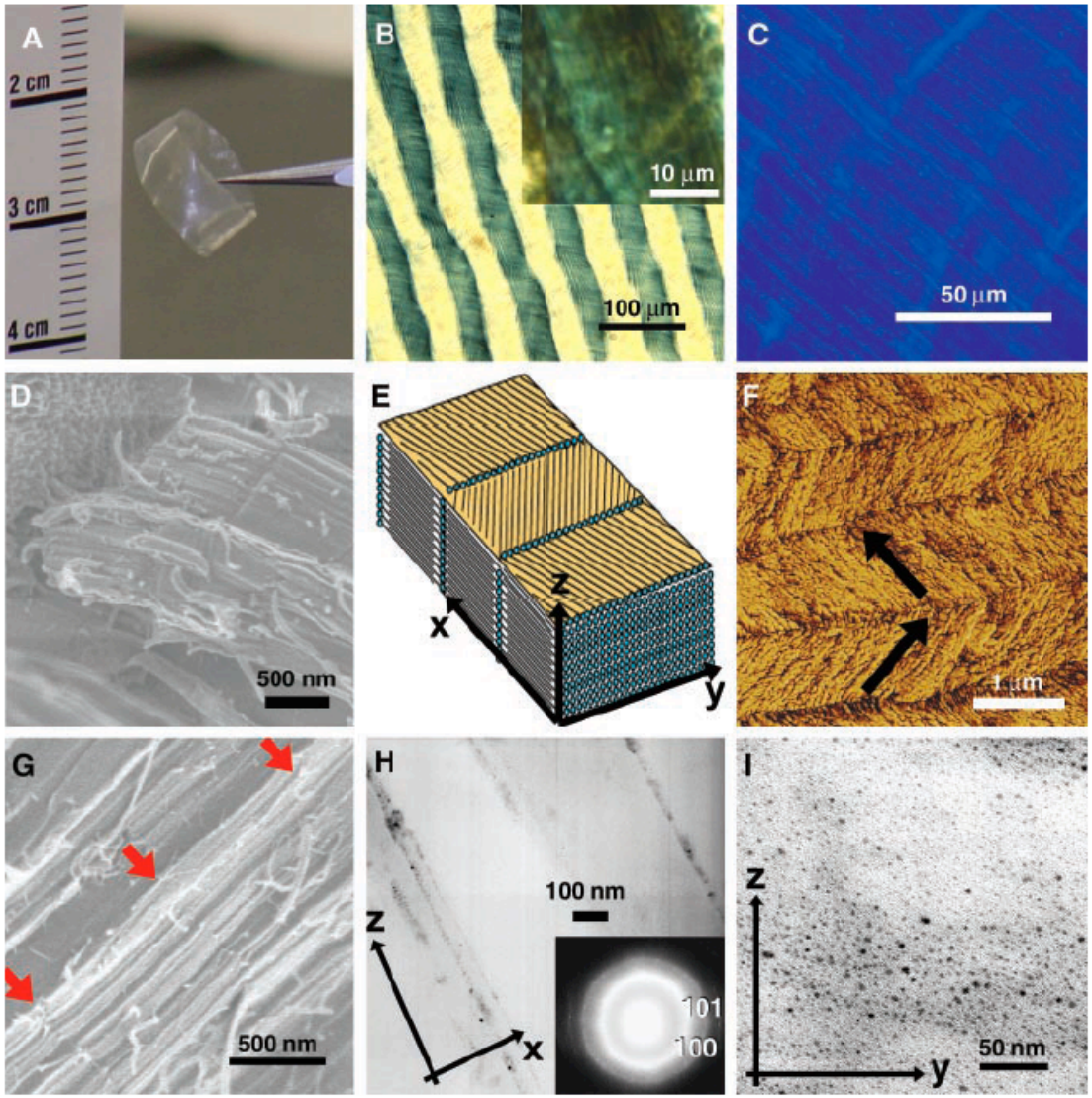

Fig. 4. Characterization of A7-ZnS film.
(**A**) Photograph of A7-ZnS viral film.
(**B**) POM (203) birefringent dark and bright band patterns (periodic length 72.8 mm) were observed. These band patterns are optically active, and their patterns reverse depending on the angles between polarizer and analyzer.
(**C**) Photoluminescent image, with an excitation wavelength of 350 nm and with filtering below 400 nm, shows ;1-mm stripe patterns (503).
(**D**) SEM images of highly packed three-dimensional bulk film structure.
(**E**) Schematic structural diagram of the A7-ZnS composite film.
(**F**) AFM image of the free surface. The phage forms parallel aligned herringbone patterns that have almost right angles between the adjacent director (arrows).
(**G**) SEM image showing the close-packed lamellar structure of phage and nanocrystal layers (red arrows) in the inner areas of the film.
(**H**) Low-resolution TEM image of cross section of A7-ZnS film, with 20 nm 3 2 mm ZnS nanocrystal stripe pattern aligned between one phage length in the *x-z* direction of film; the inset shows an electron diffraction pattern of ZnS wurtzite structure.
(**I**) Low-resolution TEM image of film viewed in the *y-z* direction, showing ZnS nanocrystals.

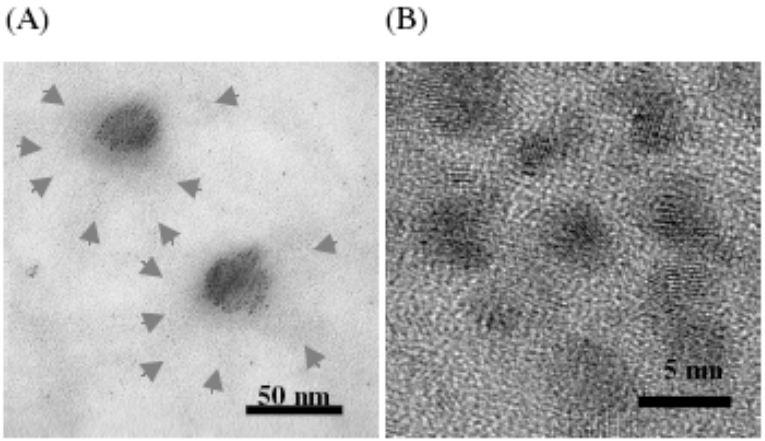

Fig. S3. (A) A micelle-like structure was visualized using 2% uranyl acetate. The ZnS nanocrystal aggregates were surrounded by phage (gray arrows). (**B**) Lattice fringe image of ZnS nanocrystal in the stained aggregate sample.

Virus-Based Toolkit for the Directed Synthesis of Magnetic and Semiconducting Nanowires

Chuanbin Mao,[1]* Daniel J. Solis,[4]* Brian D. Reiss,[5]
Stephen T. Kottmann,[4] Rozamond Y. Sweeney,[2] Andrew Hayhurst,[2]
George Georgiou,[2,3] Brent Iverson,[1,2] Angela M. Belcher[5]†

We report a virus-based scaffold for the synthesis of single-crystal ZnS, CdS, and freestanding chemically ordered CoPt and FePt nanowires, with the means of modifying substrate specificity through standard biological methods. Peptides (selected through an evolutionary screening process) that exhibit control of composition, size, and phase during nanoparticle nucleation have been expressed on the highly ordered filamentous capsid of the M13 bacteriophage. The incorporation of specific, nucleating peptides into the generic scaffold of the M13 coat structure provides a viable template for the directed synthesis of semiconducting and magnetic materials. Removal of the viral template by means of annealing promoted oriented aggregation-based crystal growth, forming individual crystalline nanowires. The unique ability to interchange substrate-specific peptides into the linear self-assembled filamentous construct of the M13 virus introduces a material tunability that has not been seen in previous synthetic routes. Therefore, this system provides a genetic toolkit for growing and organizing nanowires from semiconducting and magnetic materials.

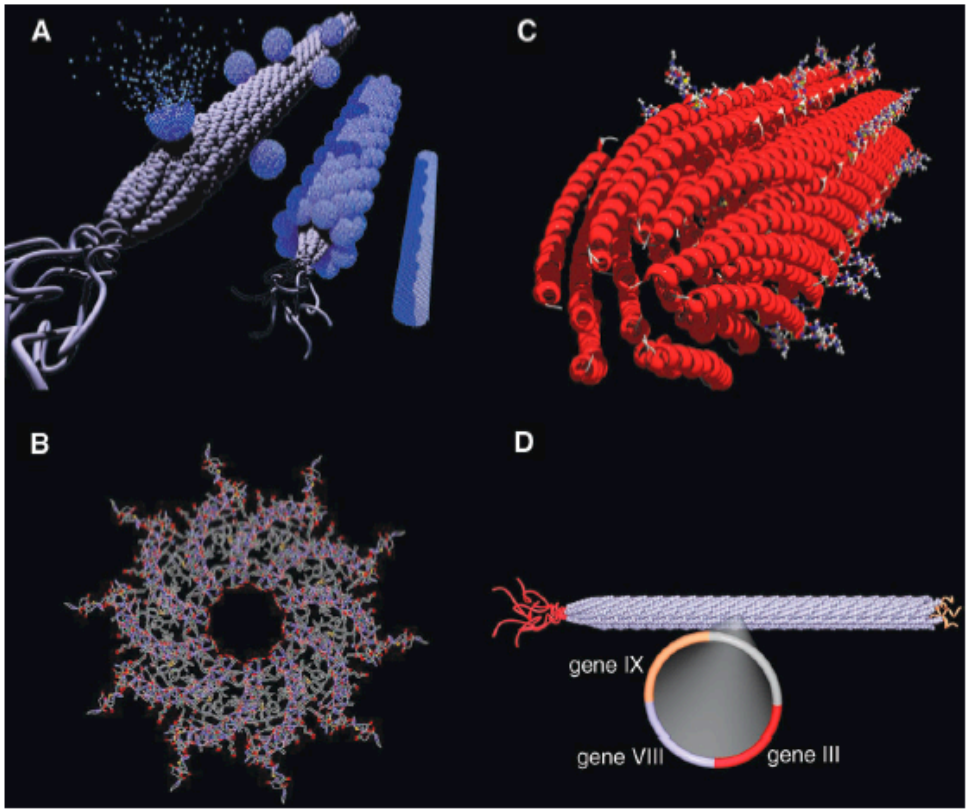

Fig. 1. Visualization of the M13 bacteriophage and the subsequent nanowire synthesis. The gP8 coat assembly was reconstructed from the x-ray fiber crystallographic data (PDB number 1ifj). The gP3 and gP9 proteins located at the proximal and remote ends of the virus are not to scale and serve as representations of the proteins. (**A**) The nanowire synthesis scheme is visualized for the nucleation, ordering, and annealing of virus-particle assemblies. (**B**) The symmetry of the virus allows for ordering of the nucleated particles along the *x*, *y*, and *z* directions, fulfilling the requirements for aggregation-based annealing. (**C**) The highly ordered nature of the self-assembled M13 bacteriophage promotes the preferred orientation seen in nucleated particles through the rigidity and packing of the expressed peptides, which is visualized at 20% incorporation. (**D**) The construct of the M13 bacteriophage virus showing the genetically modifiable capsid and ends, specifically the gP3, gP8, and gP9, which are coded for in the phagemid DNA enclosed within the virus capsid.

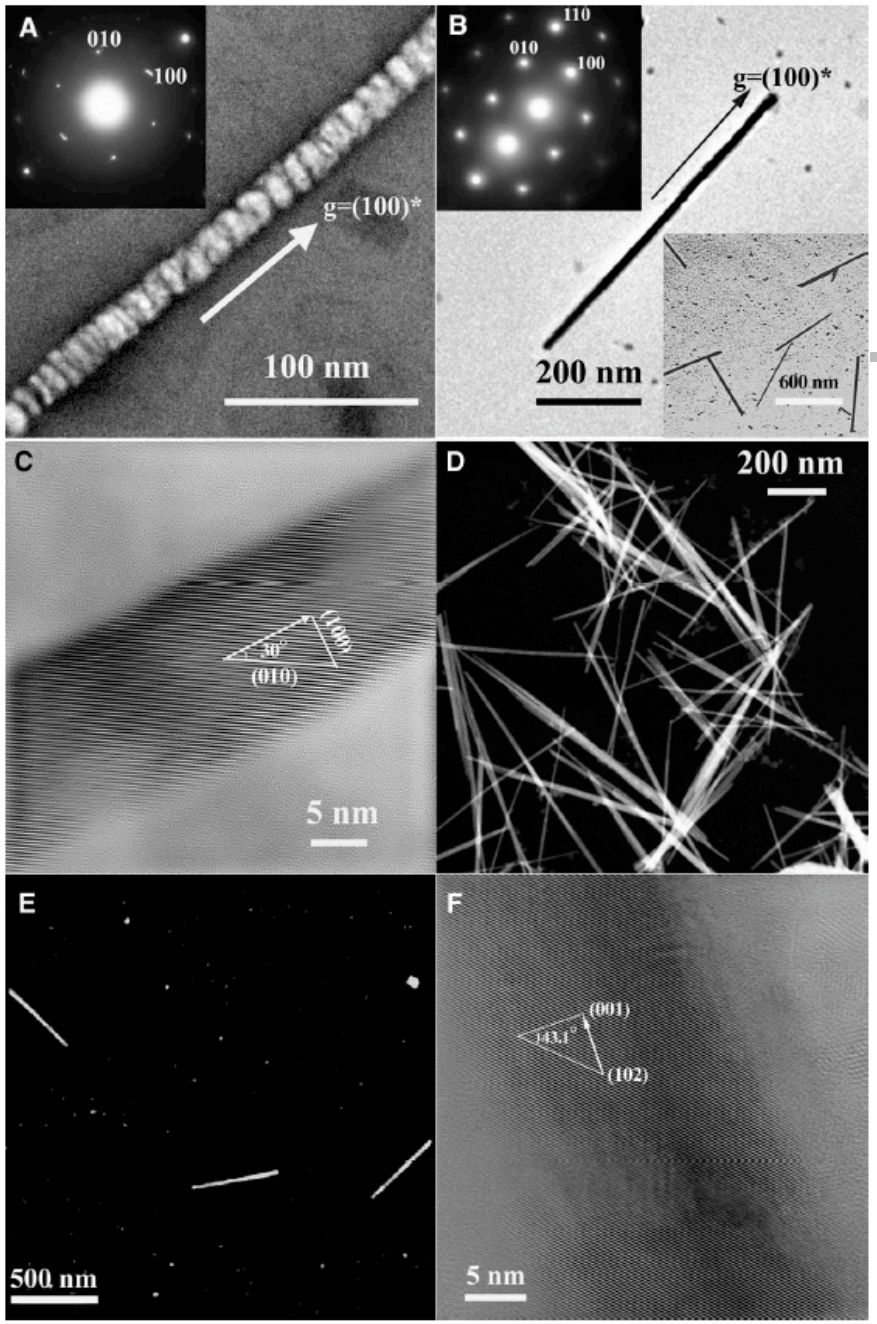

Fig. 2. Electron microscopy of both the pre- and postannealed ZnS and CdS viral nanowires. (**A**) Dark-field diffraction-contrast imaging of the pre-annealed ZnS system using the (100) reflection reveals the crystallographic ordering of the nucleated nanocrystals, in which contrast stems from satisfying the (100) Bragg diffraction condition. (Inset) ED pattern of the polycrystalline pre-annealed wire showing the wurtzite crystal structure and the single-crystal type [001] zone axis pattern, suggesting a strong [001] zone axis preferred orientation of the nanocrystals on the viral template. g = (100)* denotes the reciprocal vector of (100) crystal planes, which is perpendicular to the (100) planes and has a length inversely proportional to the interplanar spacing of the (100) planes. (**B**) Bright-field TEM image of an individual ZnS single-crystal nanowire formed after annealing. (Inset, upper left) ED pattern along the [001] zone axis shows a single-crystal wurtzite structure of the annealed ZnS nanowire. (Inset, lower right) Low-magnification TEM image showing the monodisperse, isolated single-crystal nanowires. (**C**) A typical HRTEM of a ZnS single-crystal nanowire showing a lattice image that continually extends the length of the wire, confirming the single-crystal nature of the annealed nanowire. The measured lattice spacing of 0.33 nm corresponds to the (010) planes in wurtzite ZnS crystals. A 30° orientation of (010) lattice planes with respect to the nanowire axis is consistent with the (100) growth direction determined by ED. (**D**) HAADF-STEM image of single-crystal ZnS nanowires, which were annealed on a silicon wafer. (**E**) HAADF-STEM images of CdS single-crystal nanowires. (**F**) A HRTEM lattice image of an individual CdS nanowire. The experimental lattice fringe spacing, 0.24 nm, is consistent with the unique 0.24519-nm separation between two (102) planes in bulk wurtzite CdS crystals.

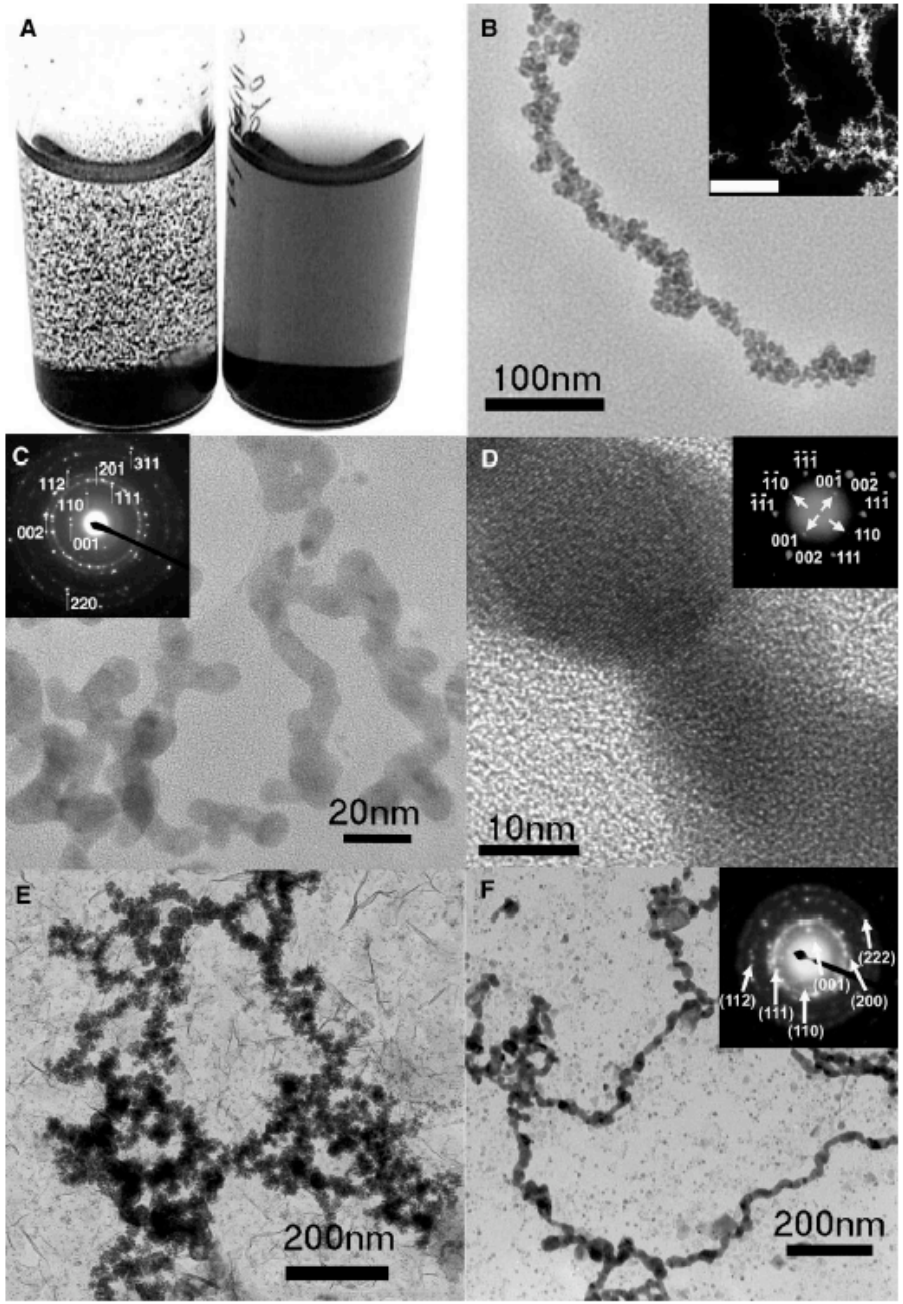

Fig. 3. (A) CoPt wires, synthesized by the modified virus template, were soluble in water (right). The reduction of Co and Pt salts without the presence of the virus yielded large precipitates which immediately fell out of solution (left). (B) TEM image of the unannealed CoPt nanoparticle-virus system. (Inset) STEM image of the unannealed CoPt wires. Scale bar, 100 nm. (C) Low-resolution TEM image of crystalline $L1_0$ CoPt wires (650 × 20 nm). The tendency of the CoPt and FePt wires not to be straight stems from magnetic interactions between wires that are not present in the II-VI systems. (Inset) ED shows the characteristic (110) and (001) $L1_0$ lines and the crystallinity of the system. (D) HRTEM of the CoPt wires with the (111) plane perpendicular to the *c* axis of the wire. (Inset) ED of an annealed CoPt wire reveals the superlattice structure unique to the $L1_0$ phase. (E) TEM imaging of the unannealed FePt wires. (F) TEM of the annealed FePt wires. (Inset) ED pattern confirming the $L1_0$ nature of the FePt wires and showing the crystalline nature of the material.

Belcher, virus ••> circuit

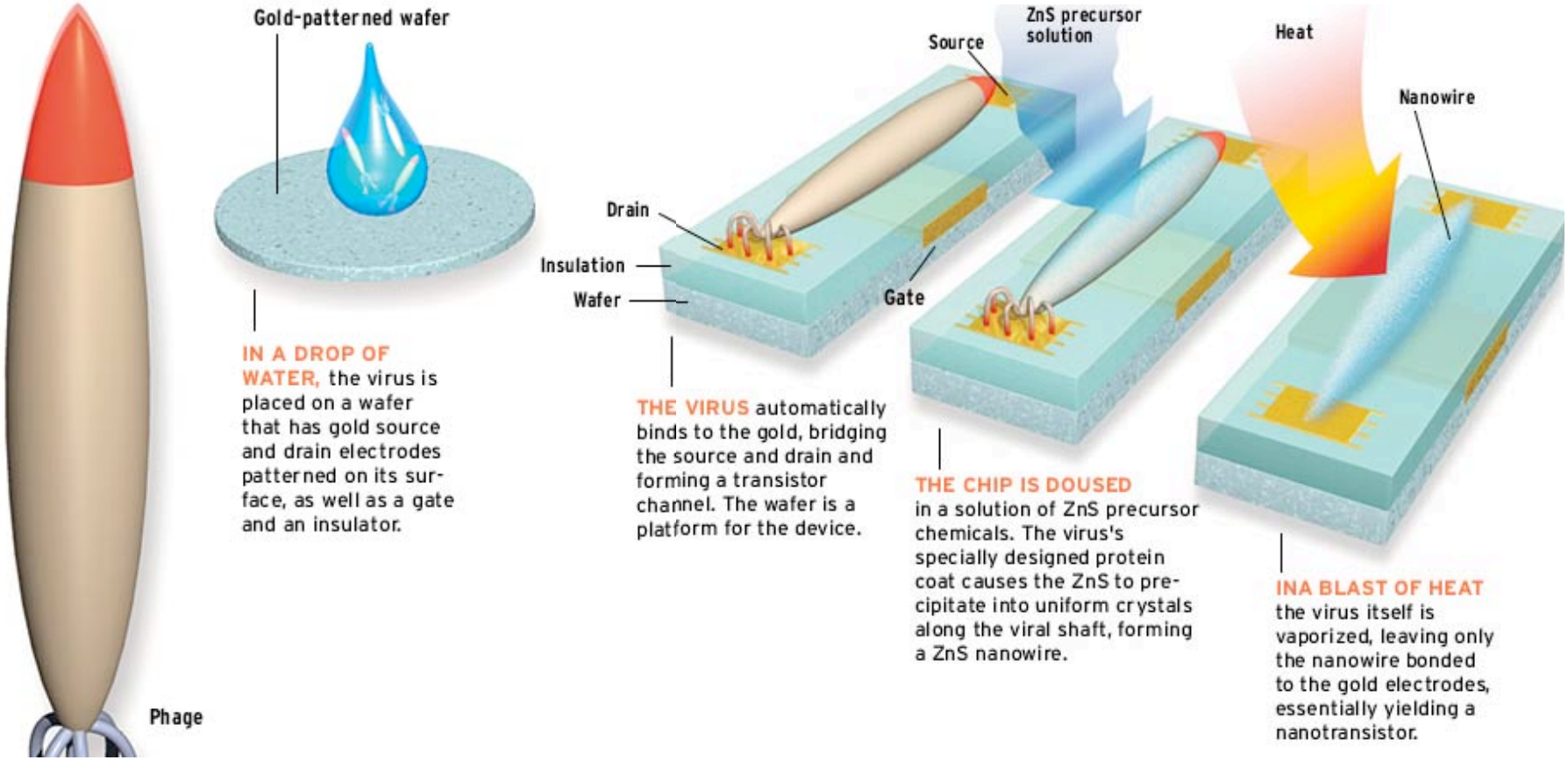

Organization of virus by LBL

Spontaneous assembly of viruses on multilayered polymer surfaces Pil J. Yoo, Ki Tae Nam, Jifa Qi, Soo-Kwan Lee, Juhyun Park, Angela M. Belcher, Paula T. Hammond

Nature Materials **5**, 234-240

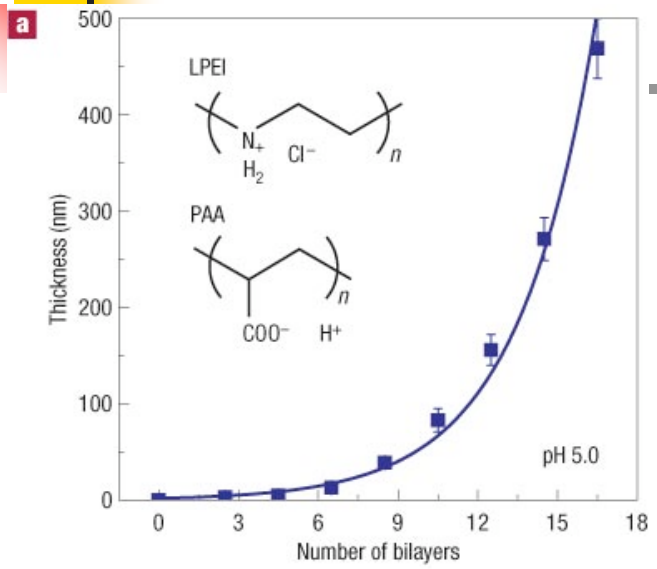

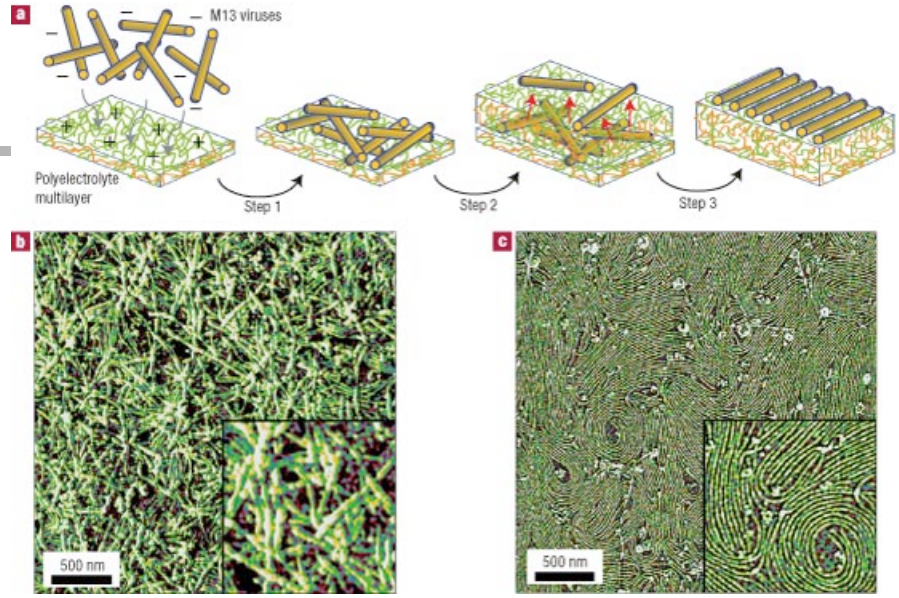

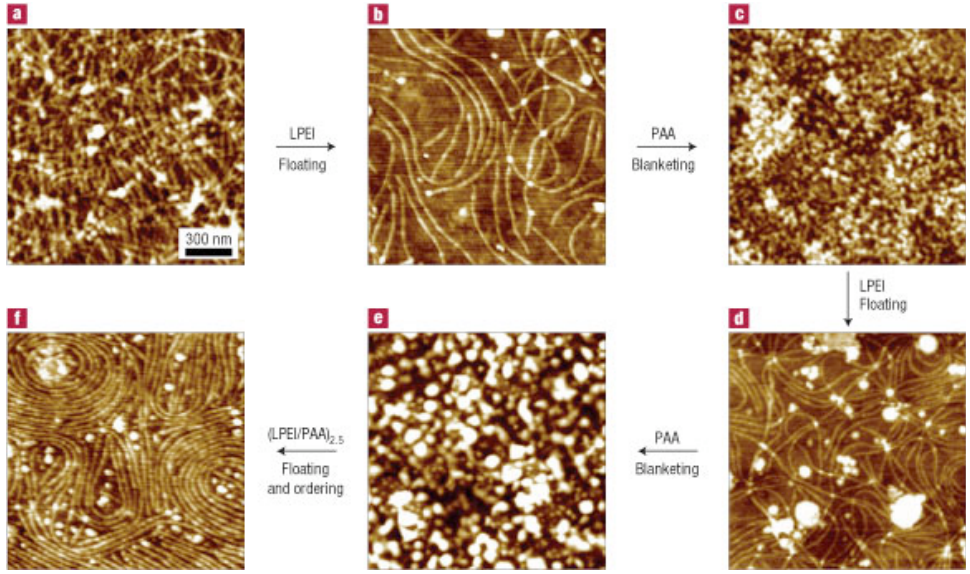

Organization of virus by LBL

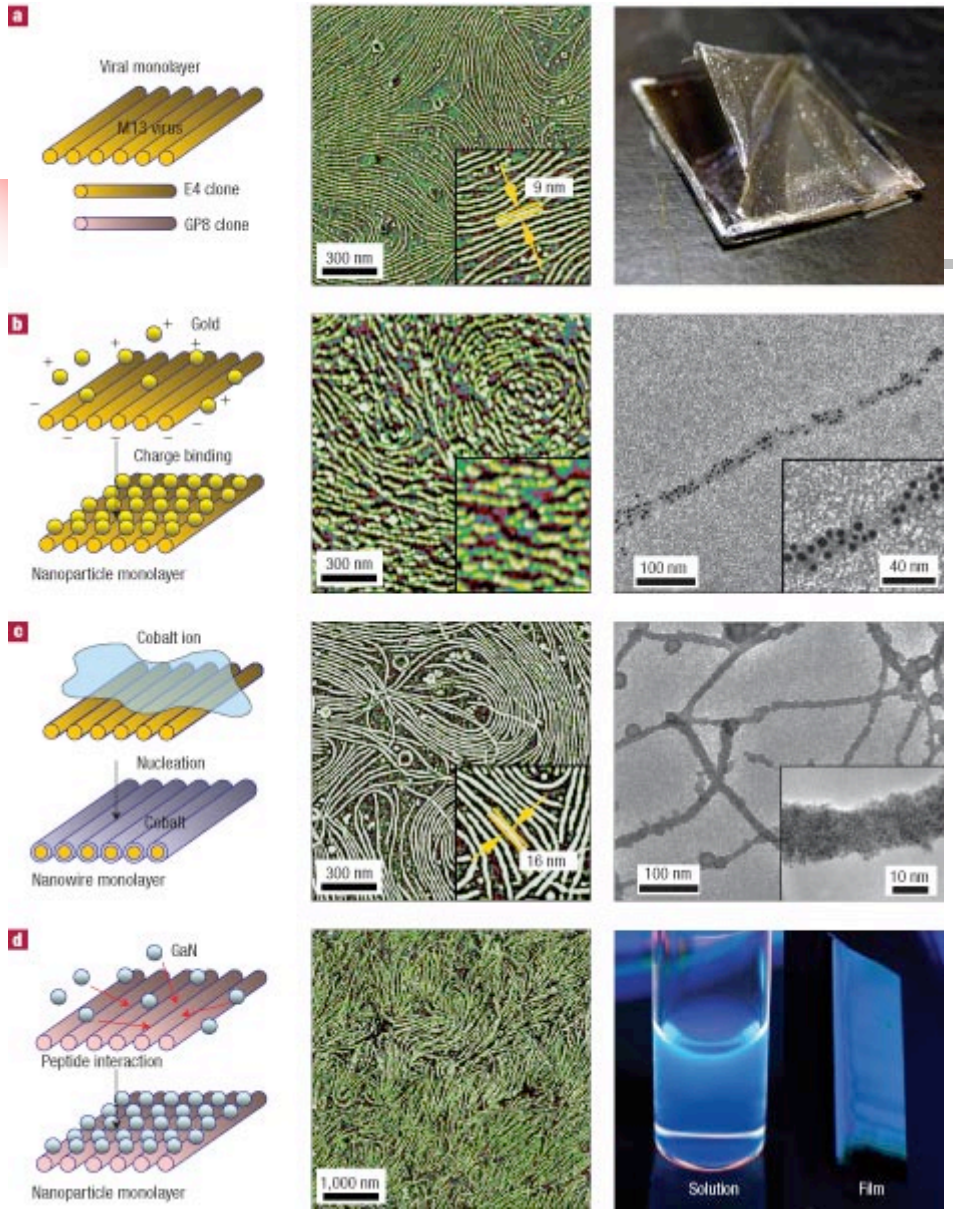

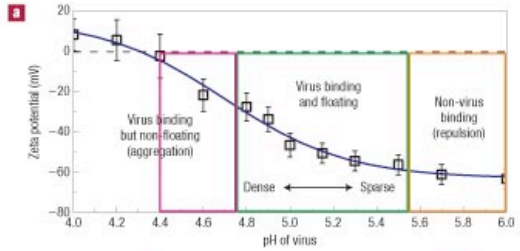

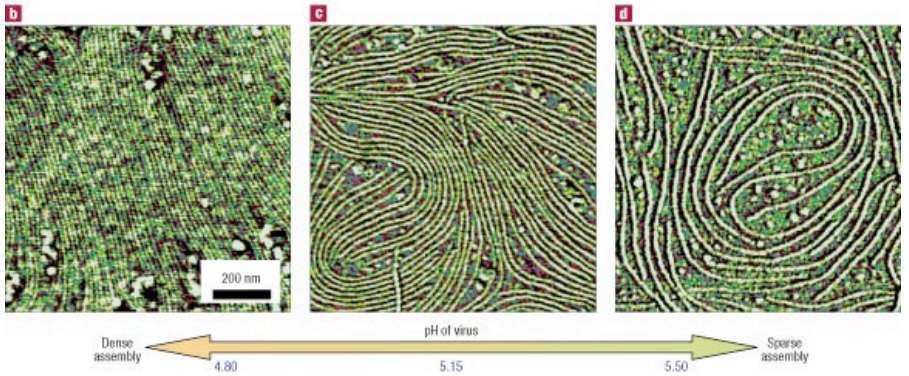

Icosahedral Virus Periodic Table

MICROBIOLOGY AND MOLECULAR BIOLOGY REVIEWS, Dec. 1999, p. 862–922 Vol. 63, No. 4
1092-2172/99/$04.00+0

Adding the Third Dimension to Virus Life Cycles: Three-Dimensional Reconstruction of Icosahedral Viruses from Cryo-Electron Micrographs

T. S. BAKER,[1]* N. H. OLSON,[1] AND S. D. FULLER[2,3]

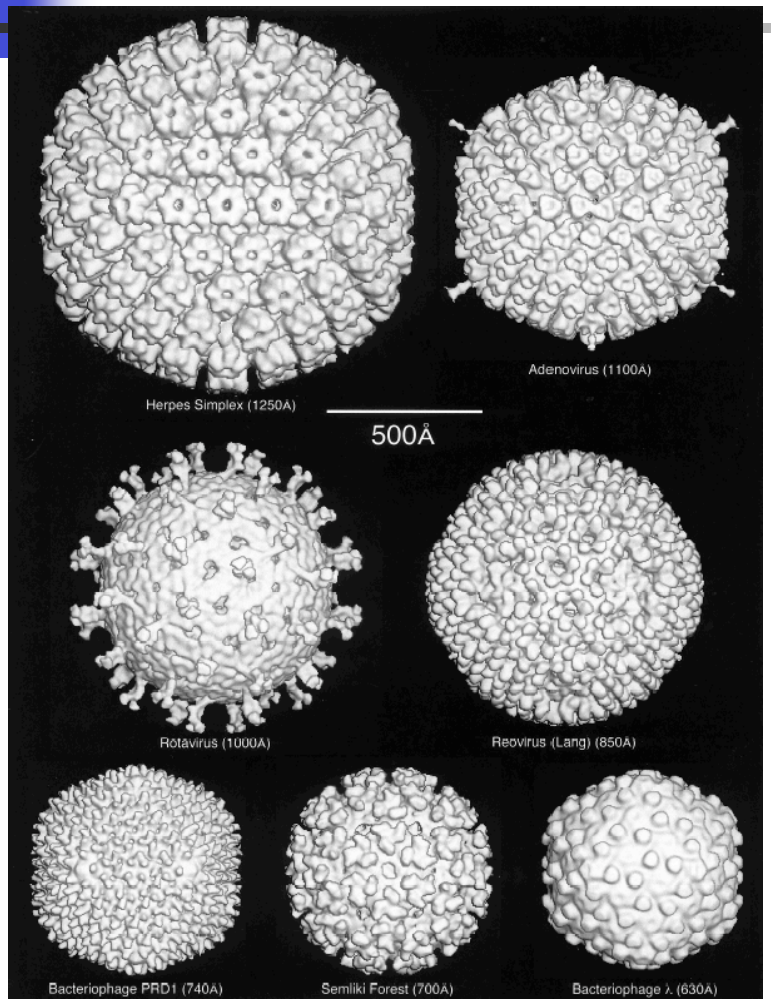

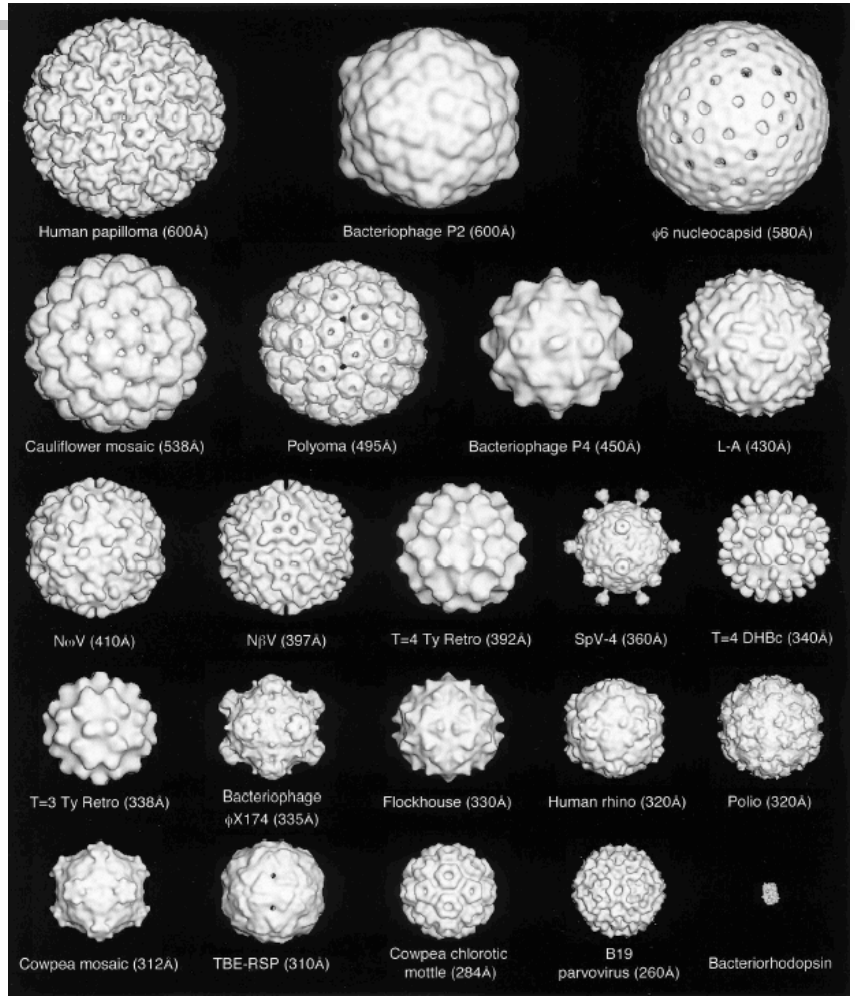

Icosahedral Virus Particles as Addressable Nanoscale Building Blocks**

Qian Wang, Tianwei Lin, Liang Tang, John E. Johnson,* and M. G. Finn*

Angew. Chem. Int. Ed. **2002**, *41*, No. 3

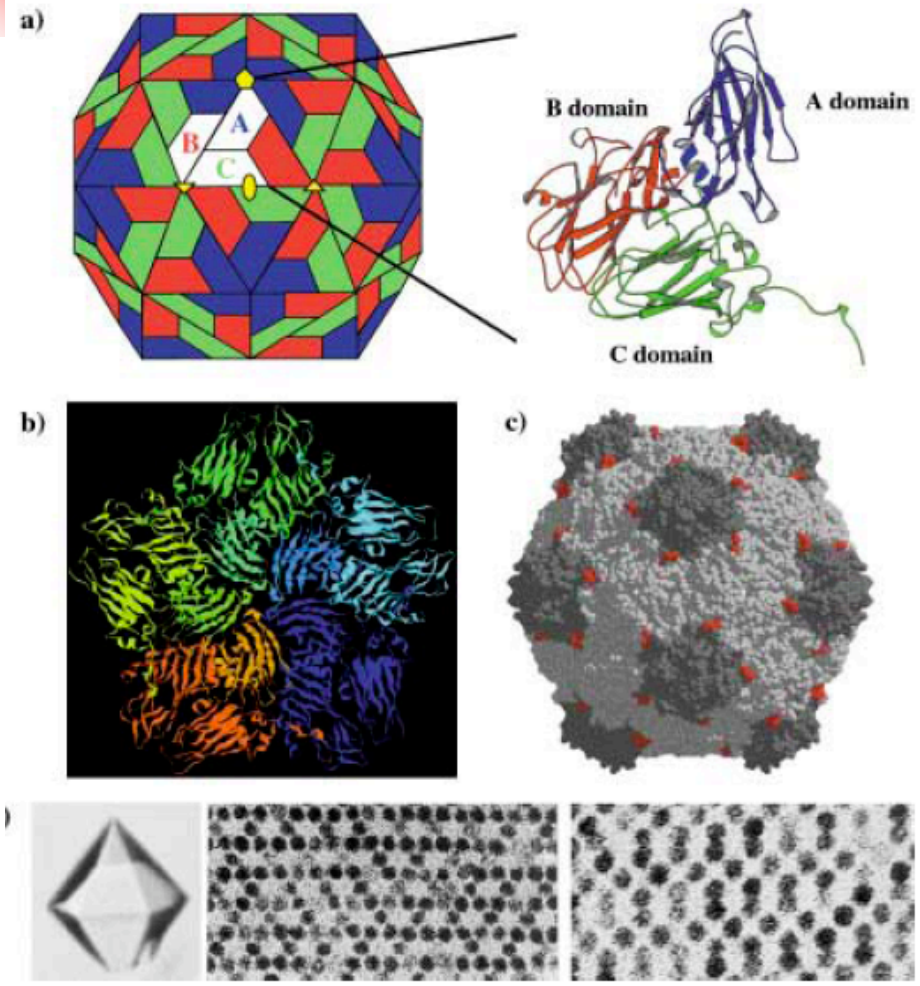

Figure 1. Structure of cowpea mosaic virus and its crystals. a) Left: A diagramatic representation of CPMV which shows the distribution of the two subunits that comprise the "asymmetric unit", 60 copies of which form the icosahedral particle. The trapezoids in red and green represent the two domains of the large subunit clustered around the threefold symmetry axes and the blue trapezoid represents the small subunit clustered about the fivefold symmetry axes. Right: The folds of the two subunits. b) Organization of five asymmetric units into the "pentamer" centered around a small hole at each fivefold axis. c) Representation of the X-ray crystal structure of CPMV that highlights the EF-loop (in red) in the large subunit in which the cysteine-containing insert is made. d) Left: A hexagonal crystal of CPMV. Electron micrographs of crystals thin sectioned perpendicular to the *c* axis (middle) and the *a* axis (right) showing the remarkably open lattice. Previous studies have shown that proteins with dimensions in excess of 50 Å can be reversibly soaked into the crystals. A typical crystal contains 10^{13} particles.

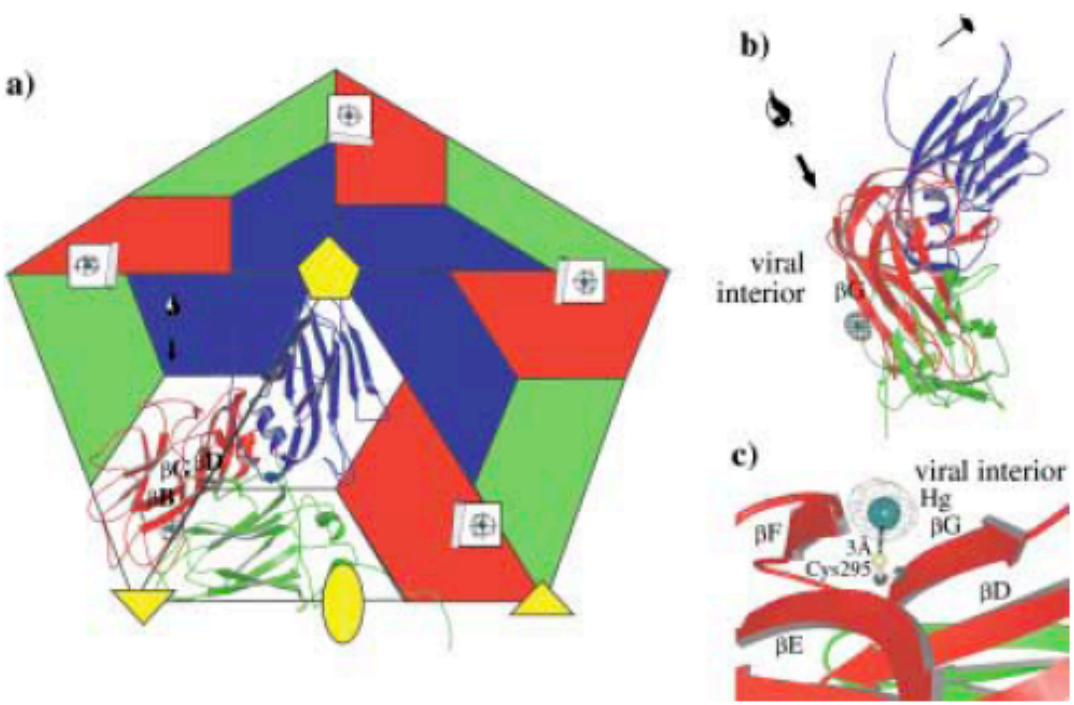

Figure 2. Crystallographic analysis of CPMV particles derivatized with EMP. Amplitudes in the Fourier series calculation were obtained by subtracting structure amplitudes computed from the atomic model of native CPMV from the measured structure amplitudes of the EMP derivative. The difference amplitudes and native phases were used to compute electron density. a) The pentameric assembly of CPMV protein about the fivefold symmetry axis. The difference electron density map reveals bound EMP molecules to be located solely at a single position below the outer capsid surface that corresponds to CYS295; five such sites are shown here. b) A view of the fold of the CPMV asymmetric unit with EMP difference density. c) A close-up view of the position of the EMP difference density.

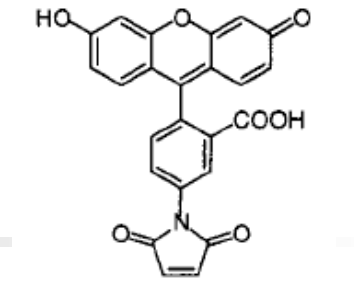

1

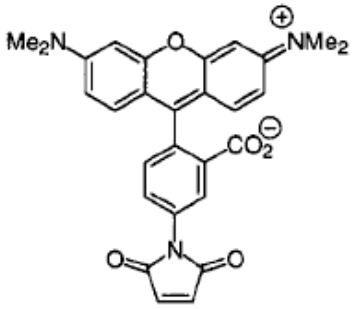

2

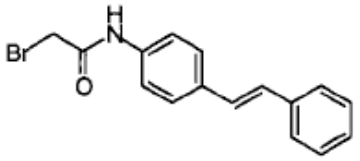

3

5-maleimidofluorescein (**1**)

5-maleimide tetramethyl- rhodamine (**2**)

stilbene derivative **3**

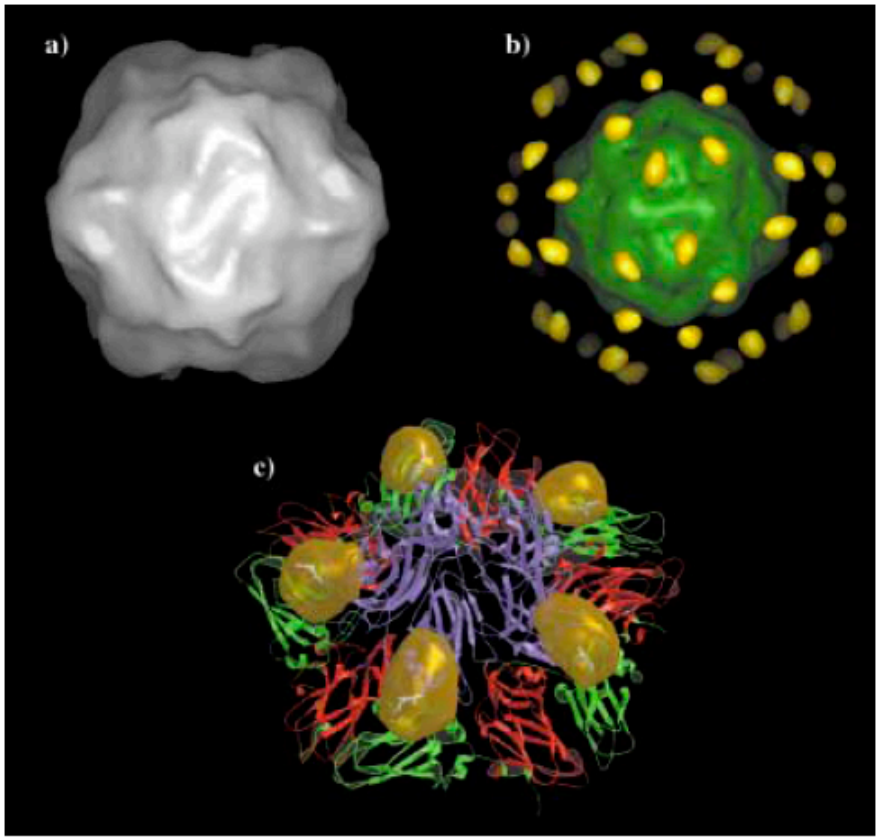

Figure 5. Cryo electron microscopy analysis of derivatized CPMV CYS mutant. a) Three-dimensional reconstruction of CPMV particles at 29 Å resolution labeled with 1.4 nm nanogold clusters. b) Difference electron density map generated by subtracting density computed with the native CPMV X-ray structure from the density shown in Figure 5a. Since the computed native CPMV density was made from only protein, the nucleic acid (shown in green) is visible in the difference map as well as the gold particles. c) A pentameric section of the difference electron density map around the fivefold symmetry axis superimposed on the atomic model of CPMV showing that the gold is attached at the site of the CYS mutation.

Nanopatterning the Chemospecific Immobilization of Cowpea Mosaic Virus Capsid

NANO LETTERS
2003
Vol. 3, No. 7
883–886

Jennifer C. Smith,[†,||] Ki-Bum Lee,[‡,||] Qian Wang,[§,||] M. G. Finn,[§] John E. Johnson,[§] Milan Mrksich,[*,†] and Chad A. Mirkin[*,‡]

Department of Chemistry and The Institute for Biophysical Dynamics, The University of Chicago, 5735 South Ellis Avenue, Chicago, Illinois 60637, Department of Chemistry and The Institute for Nanotechnology, Northwestern University, 2145 Sheridan Road, Evanston, Illinois 60208-3113, and Departments of Chemistry and Molecular Biology, The Scripps Research Institute, 10550 North Torrey Pines Road, La Jolla, California 92037

This paper presents a flexible approach for using Dip Pen Nanolithography (DPN) to nanopattern mixed monolayers for the selective immobilization of bioassemblies. DPN was used with a binary ink—consisting of a symmetric 11-mercaptoundecyl-penta(ethylene glycol) disulfide and a mixed disulfide substituted with one maleimide group—to pattern nanoscale features that present functional groups for the chemospecific immobilization of cysteine-labeled biomolecules. This strategy was applied to the chemospecific immobilization of cysteine mutant cowpea mosaic virus capsid particles (cys-VCPs). The combination of DPN for defining nanopatterns and surface chemistries for controlling the immobilization of ligands will be broadly useful in basic and applied biology.